

Article

Preparation and Characterization of Low Infrared Emissive Aluminum/Waterborne Acrylic Coatings

Xiaoxing Yan *, Lin Wang and Xingyu Qian

College of Furnishings and Industrial Design, Nanjing Forestry University, Nanjing 210037, China; wanglin@njfu.edu.cn (L.W.); qianxingyu@njfu.edu.cn (X.Q.)

* Correspondence: yanxiaoxing@nuaa.edu.cn

Received: 14 November 2019; Accepted: 27 December 2019; Published: 1 January 2020



Abstract: An aluminum/waterborne acrylic coating was developed by orthogonal experiments, and the gloss, emissivity, chromatic distortion, hardness, adhesion, impact resistance, and corrosion resistance of the coatings were examined. The results showed that the effect of drying time on the infrared emissivity of coatings was more significant than that of the Al powder concentration and nano-silica slurry. When the drying time was prolonged from 0.5 to 6.0 min, the gloss of the coating decreased slowly and the gloss remained low. The infrared emissivity first decreased and then increased. The infrared emissivity of coatings dried for 2.0 min was better. The L' value gradually decreased and showed a small change of range. With the increasing of the drying time, the hardness of the coating gradually decreased and was the highest at 0.5–2.0 min. The drying time had no effect on the adhesion level. The impact resistance of the coating was better during the drying period of 1.0–3.0 min. The corrosion resistance of the coating was better at 2.0 min. When the drying time was 2.0 min, the waterborne coating showed the better comprehensive performance. This study provides new prospects in using low infrared emissive coatings for infrared stealth and compatibility with visible light.

Keywords: drying time; aluminum/waterborne coatings; infrared emissivity; coating properties

1. Introduction

With the development of infrared technology, low infrared emissive coatings, which conceal the object from infrared detection due to their high infrared reflectivity properties, have become a new field of concern [1]. Infrared detection is widely used in military, medical, and engineering fields for its convenience and high accuracy [2]. In recent years, many researchers have conducted extensive work on infrared thermal stealth coatings. Liang et al. [3] studied the preparation and characterization of low infrared emissive color coatings based on nanometer pigment. Ji et al. [4] studied the vanadium dioxide nanopowders with tunable emissivity for adaptive infrared camouflage in both thermal atmospheric windows. Qiao et al. [5] prepared the multifunctional poly (melamine-urea-formaldehyde)/graphene microcapsules via in situ polymerization and studied the low infrared emissivity and high thermal conductivity of the MUF@graphene composites. Zhao et al. [6] prepared high-temperature-resistant coatings with low infrared emissivity by using polysiloxane resin and flake aluminum as the adhesive and pigment, respectively. Feng et al. [7] studied infrared normal spectral emissivity on quasi-periodic microstructured silicon. The above researchers focused on the tunable emissivity and high temperature resistance of infrared coatings, but less on the comprehensive properties of corrosion resistance, chromatic distortion, and gloss. Low infrared emissive coatings can achieve infrared stealth without changing the shape of military targets under existing conditions, and have been widely used in stealth technology [8]. In addition to low emissivity, infrared emissive coating also requires environmental

protection, good corrosion resistance, low gloss, low brightness, in order to facilitate visible light compatibility [9].

With the enhancement of national awareness of environmental protection [10], waterborne coatings as the new environment-friendly type of coatings, began to be advocated by the public [11]. At the moment, the waterborne coatings have found wide application in wood [12], metallic materials, and walls, etc. [13]. The term waterborne coatings refers to coatings using water as solvent or dispersing medium [14]. Waterborne acrylic based coatings use cheap and easily available water as the solvent and water evaporation does not produce any toxic atmospheres. This not only reduces the pollution to the atmosphere and improves the working environment, but also saves a lot of resources [15]. However, the corrosion resistance, hardness, and impact resistance of waterborne coatings are poor [16], and the gloss is high, which limits the application of waterborne coatings for low infrared emissivity.

To a certain extent, several fillers such as Cu powder [17], silane coupling agent [18], Al powder [19], CeO₂ powder [20], can enhance corrosion resistance, hydrophobic, mechanical properties, or wear resistance of coatings. In particular, Al powder can be used as filler in waterborne coatings to prepare coatings with low infrared emissivity and high gloss, due to its silver color, high brightness, and good adherence [21]. However, high gloss limits the application of aluminum powder for compatibility with visible light. Stringent safety measures are required to prevent dust explosions and corrosion of aluminum, which can release hydrogen gas [22]. The Al powder used in this paper was modified with oleic acid. Furthermore, the nano-silica concentrate slurry (nano-silica slurry) can reduce the gloss of coatings [23]. For this reason, it would be an ideal method to control interfacial interaction between the filler and the polymer by using nano-silica slurry to improve the corrosion resistance properties and mechanical properties in low infrared emissive coatings.

In this paper, orthogonal experiments were carried out to optimize the parameters of infrared emissive waterborne coating, such as performance formula, curing time, etc. Emphasis was laid on changing drying time. On the premise of meeting the two indices of the emissivity and gloss, the effects of infrared emissivity, chromatic distortion, gloss, mechanical properties, and corrosion resistance of waterborne coating were explored to establish a foundation for application of low infrared emissive coatings in engineering.

2. Materials and Methods

2.1. Test Materials

Waterborne acrylic coatings were provided by Yihua Living Science and Technology Co., Ltd. (Shantou, China). Waterborne acrylic coatings were composed of acrylic copolymers supported by water (the concentration was 90.0%), dipropylene glycolmethyl ether (the concentration was 2.0%), and dipropylene glycol butyl ether (the concentration was 8.0%). The solid concentration of the coating is about 26.5%. Al powder 4017 (as filler, M_w: 26.9815 g/mol, CAS No.: 7429-90-5, diameter: 10 μm, thickness: 220 nm, 65% Al powder mixed with 35% oleic acid) was supplied by Zhangqiu Metal Pigment Co., Ltd. (Zhangqiu, China). Aluminum substrate (100 mm × 50 mm × 1 mm) was provided by Shanghai Zhanchang Aluminum Industry Co., Ltd., Shanghai, China. Nano-silica slurry (particle size: 150 nm, solid concentration: 15.0%) was supplied by Suzhou Shiming Science and Technology Co., Ltd. (Suzhou, China). Anhydrous ethanol (M_w: 46.07 g/mol, CAS No.: 64-17-5) was supplied by Shandong Xinheng Chemical Co., Ltd. (Jinan, China). All reagents in the experiment were used without further processing.

2.2. Preparation of Coatings

Orthogonal experimental design is a research method of multifactors and multilevels. Orthogonal test is to select some representative points from the comprehensive test according to the orthogonality. This experimental design method is efficient, fast, and economical. In this paper, Al powder content, nano-silica slurry content, and drying time are the independent factors, which can be controlled,

respectively. The effect of Al powder and nano-silica slurry contents on the time required to fully dry the coatings is minor, and the parameter of drying time was considered independent. The effect of drying time on infrared emissivity was obtained by orthogonal experiment, and then independent experiments were carried out based on orthogonal experiment. The effects of drying time on gloss, infrared emissivity, color difference, hardness, flexibility, impact resistance, and corrosion resistance of coatings were investigated. Three factors and two levels orthogonal experiments were designed. The mass fraction of Al powder was 20.0%–40.0%, the mass fraction of nano-silica slurry was 2.0%–10.0%, and the drying time was 5.0–10.0 min in 70 °C drying environment of blast dryer. In the three-factor two-level orthogonal experiment, the variables were shown in Table 1 (sample 1#–4# for orthogonal test samples).

Table 1. Experiment arrangement and ingredients.

Sample	Al Powder (%)	Nano-Silica Slurry (%)	Drying Time (min)
1#	20.0	2.0	5.0
2#	20.0	10.0	10.0
3#	40.0	2.0	10.0
4#	40.0	10.0	5.0
5#	30.0	2.0	0.5
6#	30.0	2.0	1.0
7#	30.0	2.0	2.0
8#	30.0	2.0	3.0
9#	30.0	2.0	4.0
10#	30.0	2.0	5.0
11#	30.0	2.0	6.0
12#	30.0	0	1.0

First of all, before preparing the coating, the aluminum substrate needed to be pretreated. Firstly, sandpaper was used to polish the substrate. Secondly, oil was removed using gasoline. Thirdly, the substrate was dried in an oven. Then, Al powder and nano-silica slurry were added into waterborne coatings according to the predesigned amount in Table 1, mixed, and stirred evenly. Furthermore, it was coated using SZQ tetrahedral fabricator (Tianjin Jinghai Science and Technology Testing Machinery Factory, Tianjin, China) onto the pretreated aluminum substrate (100 mm × 50 mm × 1 mm). The substrate was fixed on the platform. Then, the prepared coating was poured in front of the fabricator. The two ends of fabricator were grasped by hand, then glided at 150 mm/s, so that the required thickness of the coating could be coated. It was firstly dried at room temperature for 3 h to obtain the surface dry state, then dried in 70 °C blast dryer for 0.5–10.0 min, and then cooled to room temperature. About 60 µm thick dry waterborne coating was used for comparison. In order to study the key influence of drying time on infrared emissivity, a series of independent experiments were carried out on the basis of orthogonal experiment. The concentration of Al powder was fixed at 30.0%, the concentration of nano-silica slurry was fixed at 2.0%, and the drying time was changed to 0.5, 1.0, 2.0, 3.0, 4.0, 5.0, and 6.0 min, respectively. Samples 5#–11# prepared for independent experiments were shown in Table 1. The sample 12# without nano-silica slurry was prepared for comparison of gloss, showing that nano-silica slurry can decrease the gloss of coatings.

2.3. Performance Test

The details of the experimental test equipment are shown in Table 2. The thickness of dry coating was measured by JKTH-1250B digital coating thickness gauge. The microstructure of coating was observed by Quanta 200 environment scanning electron microscope (SEM). Vertex 80V infrared spectrum analyzer was used to determine the functional group changes of the coatings at different curing time. The far infrared emissivity of the coatings in the range of 8–14 µm was measured by IR-2 infrared emissive tester. The measurement error of the far infrared emissivity is less than 0.001. The

gloss of coatings was measured with a HG268-60° gloss meter. In the impact test, the coating is placed on the anvil at the bottom of the instrument, and then the hammer is lifted to a certain height and is dropped freely to impact the sample. The magnifying glass is observed to judge whether the coating has cracks, wrinkles, and peeling. If there is any damage, it is considered as unqualified at this height. If there is no damage, it is considered as qualified at this height. When measuring the adhesion of coating, the tip of the rotary needle touches the coating, and the handle is shaken uniformly clockwise at 80–100 r/min, and the scratch length of the circular roller is 7.5 ± 0.5 cm. At the end of the adhesion test, the damage to the coating was observed using a magnifier. The marks 0, 1, 2, 3, 4, 5, 6, and 7 on the top of the coating are the eight levels of damage. The adhesion of level 0 was the strongest, and that of level 7 was the weakest. The hardness of the coating was tested with a 6H–6B pencil. In this experiment, the angle between the pencil and the coating was 45° , and the pencil scratched under 1.0 kg load. The hardness of the film was measured under the circumstance of scratches appearance on the coatings. The color difference of coating was measured by the SEGT-J color difference meter. The flexibility of coating was measured by QTX film flexibility tester. The corrosion resistance of coating was measured by CHI660E electrochemical workstation. The concentration of NaCl was 3.5% at room temperature. Three-electrode battery structure was used for electrochemical testing. The saturated calomel electrode serves as the reference electrode and the platinum electrode serves as the counter electrode. Each sample was immersed in 3.5% NaCl solution for 30 min and the open circuit potential (OCP) was monitored until constant. The polarization test started at OCP-0.3V and stopped at OCP+0.3V with the scan rate of 0.01V/s. The software being carried by CHI660E electrochemical workstation was used to calculate the value of polarization resistance (R_p). All the experiments were repeated four times with an error of less than 5.0%.

Table 2. Experimental test equipment.

Property	Standard	Equipment	Producer
Thickness	–	JKTH-1250B digital coating thickness gauge	Tianjin Jingke Material Testing Machine Factory, Tianjin, China.
Microstructure	–	Quanta 200 environment scanning electron microscope	FEI Company, Hillsboro, Oregon, USA
Functional group changes	–	Vertex 80V infrared spectrum analyzer	Germany Bruker Co., Ltd., Karlsruhe, Germany
Far infrared emissivity	–	IR-2 infrared emissive tester	Shanghai Institute of Technological Physics of the Chinese Academy of Sciences, Shanghai, China
Gloss	GB/T 9754-2007 [24]	HG268-60° gloss meter	Shenzhen SNH Technology Co., Ltd., Shenzhen, China
Impact resistance	GB/T 1732-93 [25]	QCG-50 impulse tester	Tianjin Jingkelian Material Testing Machine Co., Ltd., Tianjin, China
Adhesion	GB/T 1720-79(89) [26]	QFZ-II circle-cut coating adhesion tester	Tianjin JingKelian Material Testing Machine Co., Ltd., Tianjin, China
Hardness	GB/T 6739-2006 [27]	6H-6B pencil	China First Pencil Co., Ltd., Shanghai, China
Color difference	GB/T 3181-1995 [28]	SEGT-J color difference meter	Guangzhou Standard Geda Laboratory Instruments Co., Ltd., Guangzhou, China
Flexibility	GB/T 1731-93 [29]	QTX film flexibility tester	Beijing Aerospace Huayu Test Instrument Co., Ltd., Beijing, China
Corrosion resistance	GB/T 15748-2013 [30]	CHI660E electrochemical workstation	Beijing Huake Putian Technology Co., Ltd., Beijing, China

3. Results and Discussion

From the analysis of range and variance in Table 3 and the influence factors of orthogonal experiment in Figure 1, the influence of drying time on infrared emissivity of coatings was more obvious than that of Al powder concentration and nano-silica slurry concentration. When the nano-silica slurry was 2.0%, the infrared emissivity was low. F-test (Table 4) showed that the three factors had no significant effect. According to Table 3, the optimum level combination was as follows: The concentration of Al powder was 40.0%, the concentration of nano-silica slurry was 2.0%, and the drying time was 5.0 min. Al powder concentration was too low which would lead to higher emissivity of coatings. Due to the strong reflectivity and gloss of Al powder, high concentration of Al powder will lead to higher gloss of coatings, which is not conducive to compatibility with visible light [31]. Therefore, 30.0% of Al powder was selected for comprehensive performance, and the concentration of Al powder was fixed to 30.0% in the following independent experiments. The optical, mechanical, chromatic distortion, and corrosion resistance of coatings were also studied.

Table 3. Orthogonal experimental analysis.

Sample	Al Powder (%)	Nano-Silica Slurry (%)	Drying Time (min)	Infrared Emissivity
1#	20.0	2.0	5.0	0.279
2#	20.0	10.0	10.0	0.473
3#	40.0	2.0	10.0	0.358
4#	40.0	10.0	5.0	0.291
k ₁	0.376	0.319	0.285	–
k ₂	0.325	0.382	0.415	–
Range (R)	0.051	0.063	0.130	–
Variance	0.0026	0.0040	0.0169	–

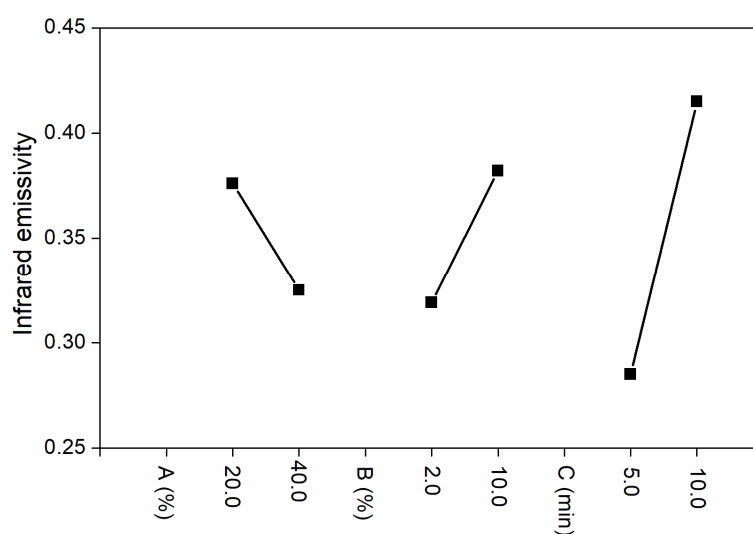


Figure 1. Orthogonal experimental effects of (A) Al powder, (B) nano-silica slurry concentration, and (C) drying time.

Table 4. F-test.

Factor	Sum of Squares of Deviations	Freedom	F Ratio	F Critical Value	Significance
Al powder (%)	0.003	1	1.000	39.900	–
Nano-silica slurry (%)	0.004	1	1.333	39.900	–
Drying time (min)	0.017	1	5.667	39.900	–

Figure 2 shows the influence of drying time on the infrared spectra of coatings. The absorption peak of wave number 3450 cm^{-1} is $-\text{OH}$ stretching vibration peak. With the prolongation of drying

time, the $-OH$ stretching vibration peak weakened, which indicated that the solvent water evaporated gradually. The peaks at 2950 cm^{-1} are the asymmetric and symmetric stretching vibration peaks of CH_3 and CH_2 in waterborne acrylic coatings. The peaks at 1724 cm^{-1} belongs to $C=O$ absorption of carboxyl in waterborne acrylic coatings. As shown in Figure 2, when the drying time was 30 s, 2.0 and 5.0 min, the infrared peaks of the coatings were basically similar. This showed that the drying time had little influence on the infrared peak of the coating and did not affect the composition of the polymer in the coating.

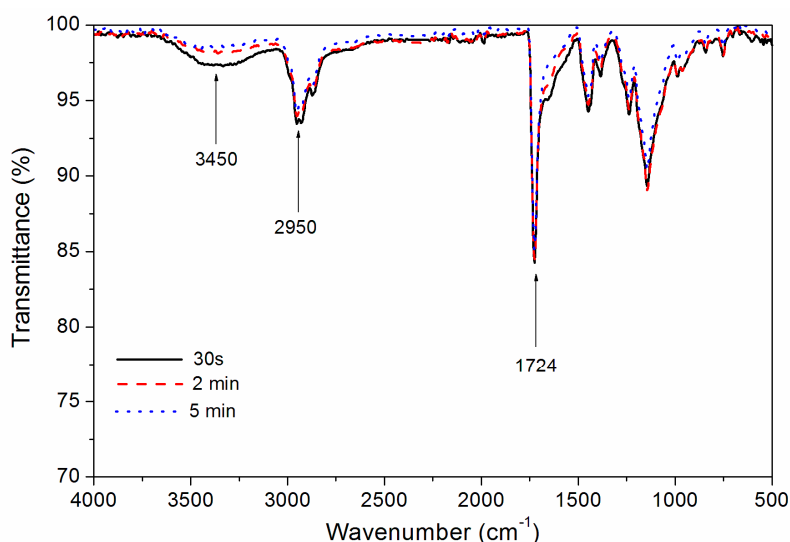
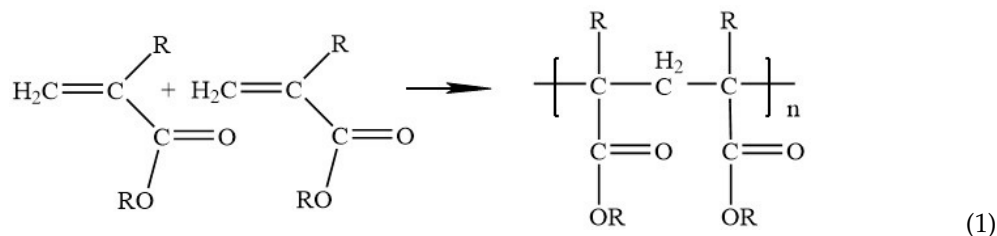


Figure 2. Effect of drying time on infrared spectrum of the coating.

The effect of drying time on the gloss of waterborne curing coatings is shown in Figure 3. The gloss of coating decreased with the increase of drying time. When the time was prolonged from 0.5 to 6.0 min, the gloss of coatings decreased from 8.1% to 6.9%, but the overall gloss remained low. For the low infrared emissive coating, the lower the gloss, the better the coating. When the drying time was 6.0 min, the gloss of was the lowest, which was 6.9%. The chemical structure of waterborne acrylic resin and the corresponding chemical reaction are shown in Equation (1). The moisture in the waterborne coating evaporated gradually, the degree of curing and crosslinking of the coating strengthened according to Equation (1), the reflectivity of the coating to visible light weakened gradually, and the gloss of coating was gradually decreased. The effect of nano-silica slurry on the gloss of coating is shown in Table 5. The sample 12# was coated without nano-silica slurry, and its gloss was higher than that of sample 6# with nano-silica slurry, which indicated that nano-silica slurry can reduce the gloss of coatings. High gloss is not conducive to compatibility with visible light, so the low gloss obtained by adding nano-silica slurry was better.



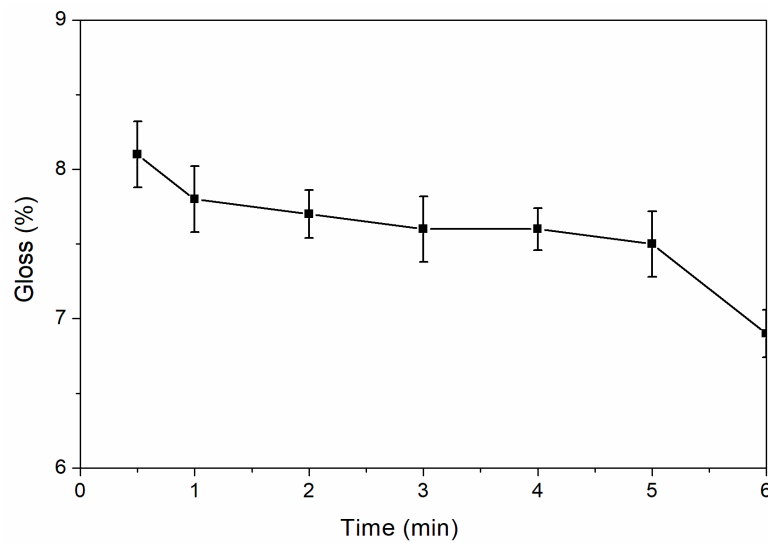


Figure 3. Effect of drying time on gloss of the coating.

Table 5. Effect of nano-silica slurry on gloss of the coating.

Sample	Nano-Silica Slurry (%)	Gloss (%)
6#	2.0	7.8
12#	0	14.1

Figure 4 shows the influence of drying time on infrared emissivity of waterborne coatings. The infrared emissivity of waterborne coatings tends to be U-shape with the increase of drying time in Figure 4. When the time increased from 0.5 to 2.0 min, the infrared emissivity of waterborne coatings decreased from 0.242 to 0.113. As the drying time continued to increase from 2.0 to 6.0 min, the infrared emissivity of waterborne coatings increased slowly from 0.113 to 0.268. Therefore, when the drying time was 2.0 min, the waterborne coating had the lowest infrared emissivity. In the period of 0.5 to 2.0 min, the addition of nano-silica slurry helped to cure the coating, reduced the thickness of the surface resin, weakened its absorption of far infrared ray, and decreased the emissivity of coating. However, after 2.0 min, continuous heating may lead to the oxidation of Al powder in the coating, so the infrared emissivity of coating began to increase. The infrared emissivity of coatings dried for 2.0 min was better.

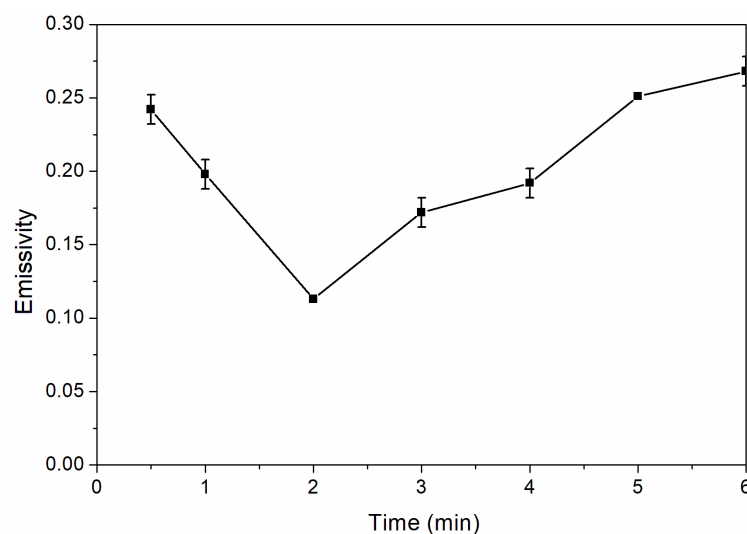


Figure 4. Effect of drying time on infrared emissivity of the coating.

Chromatic distortion is the value of color when polychromatic light is used as a light source. L , a^* , b^* represent the black and white, red and green, yellow and blue values of Al substrates, respectively. L' , $a^{*'}$, $b^{*'}$ represent the black-white, red-green, yellow-blue values of the coated substrate surface, respectively. After subtraction, the brightness difference ΔL , the red-green index difference Δa^* , the yellow-blue index difference Δb^* , and the color difference ΔE can be calculated based on Equation (2):

$$\Delta E = \sqrt{(\Delta L)^2 + (\Delta a^*)^2 + (\Delta b^*)^2} \quad (2)$$

The results of the effect of drying time on the chromatic distortion and color difference ΔE of coatings are shown in Table 6. The color difference ΔE and the brightness L' of waterborne coatings decreased gradually with the increase of drying time and the variation range was small. When the drying time increased from 0.5 to 6.0 min, the L' value of waterborne coatings decreased from 80.8 to 78.8. As the time went on, the polymer in the coating was continuously cross-linked to form a network, which was equivalent to increasing the concentration of the coating to some extent, that was, reducing the L' value [32].

Table 6. Effect of drying time on color difference of the coating.

Time (min)	L	a^*	b^*	L'	$a^{*'}$	$b^{*'}$	ΔL	Δa^*	Δb^*	ΔE
0.5	25.9	5.2	−3.1	80.8	3.4	−6.8	−54.9	1.8	3.7	55.1
1.0	25.9	5.2	−3.1	80.5	3.2	−7.1	−54.6	2.0	4.0	54.8
2.0	25.9	5.2	−3.1	79.4	3.1	−6.8	−53.5	2.1	3.7	53.7
3.0	25.9	5.2	−3.1	79.4	3.0	−6.3	−53.5	2.2	3.2	53.6
4.0	25.9	5.2	−3.1	79.3	3.4	−7.0	−53.4	1.8	3.9	53.6
5.0	25.9	5.2	−3.1	79.2	4.6	−7.8	−53.3	0.6	4.7	53.5
6.0	25.9	5.2	−3.1	78.8	2.8	6.0	−52.9	2.4	−9.1	53.7

The influence of drying time on the hardness of coating is shown in Figure 5. When the drying time is 0.5–2.0 min, the hardness of coating was the highest, which was 6H. When the drying time was over 2.0 min, the hardness of coating decreased to 4H. This is supposed to be the degree of polymer crosslinking of the coatings that was appropriate in the period of 0.5–2.0 min. When the drying time was 0.5–6.0 min, the adhesion level of the coating was better, which was level 0 (Figure 6). This is supposed to be the drying time of 0.5–6.0 min that had no effect on the adhesion level. Figure 7 shows the influence of drying time on flexibility of coatings. The flexibility of coatings decreased from 5.0 to 2.0 mm. Figure 8 shows the influence of coating drying time on impact resistance. According to Figure 8, when the drying time was 1.0–3.0 min, the impact resistance of the coating was better, which was 15.0 kg·cm. The impact resistance of coating decreased with drying time prolonging. The reason was that the coating polymer had a suitable degree of crosslinking during the drying period of 1.0–3.0 min.

The colorimetric tests, mechanical, and optical properties showed that coatings had the better properties at 1.0 and 2.0 min. Consequently, the corrosion resistance of two coatings was tested to further explore the changes of their corrosion resistance. The electrochemical polarization curves are shown in Figure 9, and the corrosion parameters obtained from Figure 9 are shown in Table 7. The porosity of coating plays a significance role in corrosion resistance. The porosity (P) of aluminum/waterborne acrylic coating can be calculated according to Equation (3):

$$P = \frac{R_{PS}}{R_{PC}} \times 10^{-(\Delta E_{corr} / \beta_{as})} \quad (3)$$

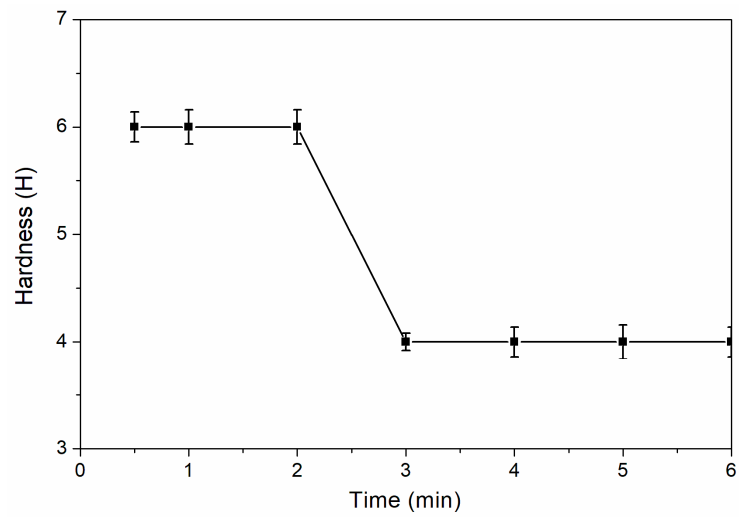


Figure 5. Effect of drying time on hardness of the coating.

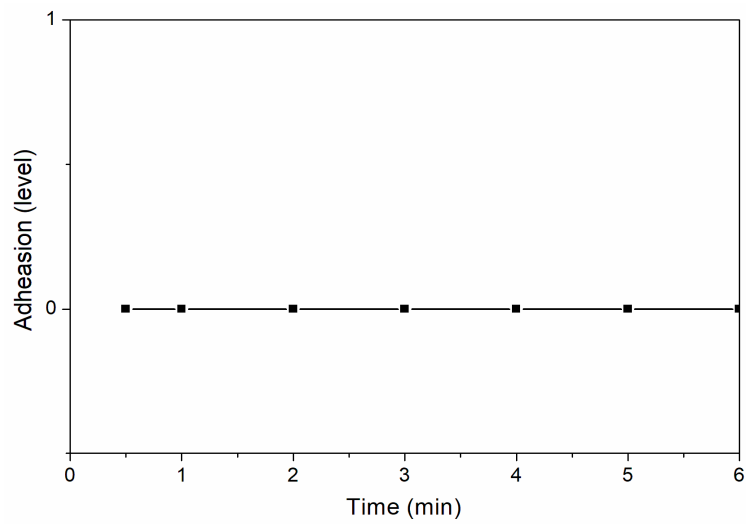


Figure 6. Effect of drying time on adhesion of the coating.

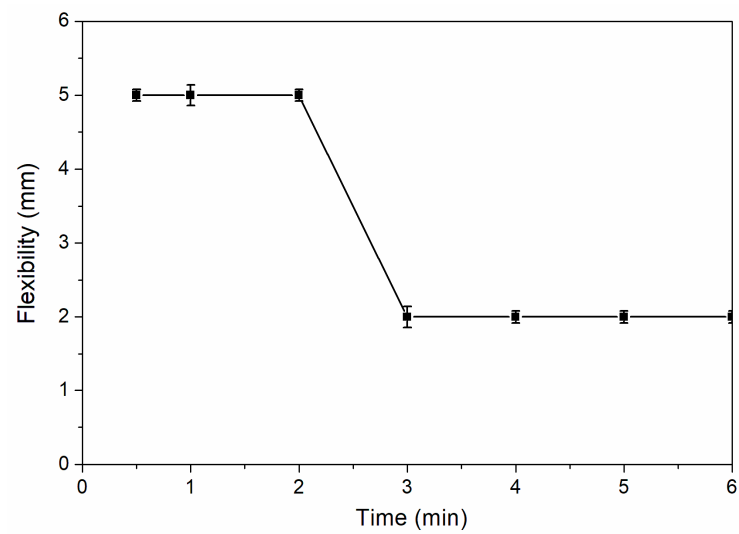


Figure 7. Effect of drying time on flexibility of the coating.

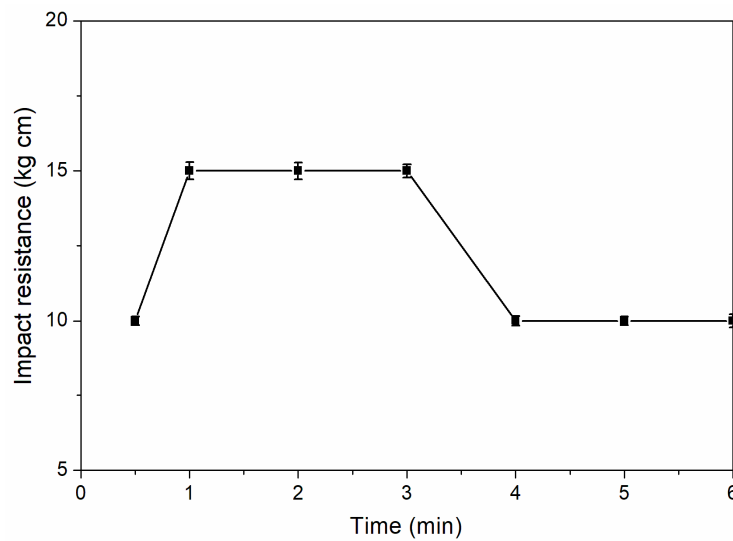


Figure 8. Effect of drying time on impact resistance of the coating.

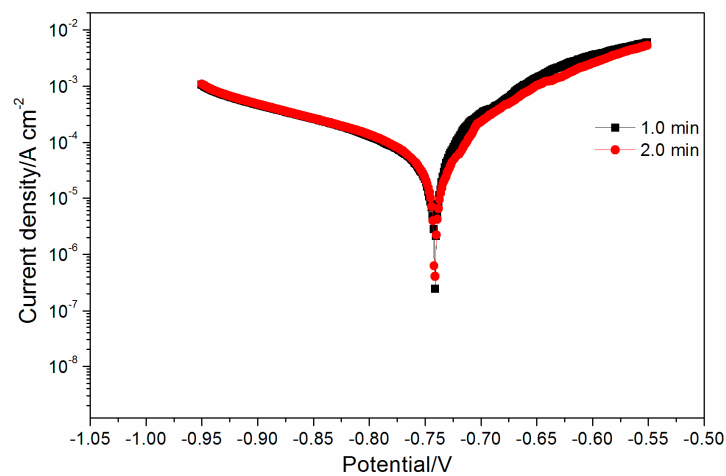


Figure 9. The electrochemical curve of the coating at drying time of 1.0 and 2.0 min.

Table 7. Effect of drying time on corrosion resistance of the coating.

Time (min)	E_{corr} (V)	R_p (Ω/cm^2)	I_{corr} (A/cm^2)	β_a (mV/dec)	β_c (mV/dec)	p
Aluminum substrate	-0.745	133.2	2.337×10^{-4}	99.69	250.44	–
1.0	-0.741	337.8	7.438×10^{-5}	86.75	173.10	0.36
2.0	-0.741	407.3	6.893×10^{-5}	99.91	183.00	0.30

In Equation (3), R_{PS} and R_{PC} are polarization resistance of the substrate and coated substrate, respectively. ΔE_{corr} is the corrosion potential difference between the coating and aluminum substrate, and β_{as} is the anode constant of aluminum substrate. In Table 7, E_{corr} is the corrosion potential, I_{corr} is the corrosion current density, R_p is the polarization resistance, and β_a and β_c are anode constant and cathode constant, respectively. Table 7 showed that when the drying time was 1.0 min, the waterborne coating had lower R_{PC} , higher I_{corr} , and higher porosity. The low porosity can decrease the NaCl solution penetration. Therefore, compared with 1.0 min, when the drying time was 2.0 min, the coating had better corrosion resistance. From Figure 10, it can be seen that the morphology of the coating after drying at different times had little change. Compared with other drying times, when the drying time was 1.0 and 2.0 min, the distribution of Al powder in the coating was more uniform, and the spacing between particles was smaller.

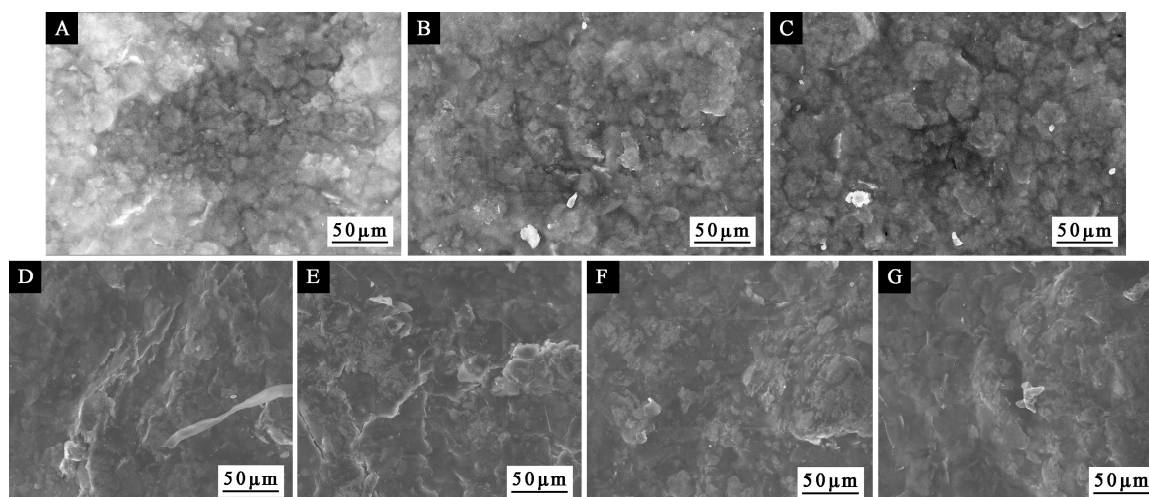


Figure 10. SEM of coating with different drying times: (A) 30 s, (B) 1.0, (C) 2.0, (D) 3.0, (E) 4.0, (F) 5.0, and (G) 6.0 min.

The performance of waterborne acrylic based coating was compared with that of the PU based coating [33–35] and epoxy-lacquer based coatings [36], as shown in Table 8. Compared with other coatings, the infrared emissivity of aluminum/waterborne acrylic coating can reach a low value of about 0.1. The gloss of aluminum/waterborne acrylic coating is lower than that of PU-based coatings, which is similar to that of epoxy-lacquer based coatings. The adhesion of aluminum/waterborne acrylic coating is the highest, which is level 0. The porosity (p) of the aluminum/waterborne acrylic coating is the largest, which is 0.3. The impact resistance and corrosion resistance of low infrared emissive aluminum/waterborne acrylic coating are worse than low infrared emissive PU/(ball-milled Ag-Cu) [33], PU/Al coatings [35] and epoxy-lacquer/Al [36].

Table 8. Performance comparison of waterborne acrylic based coating with PU based coatings and epoxy-lacquer based coatings.

Coating	Filler Mass Fraction (%)	Emissivity	Gloss (%)	Adhesion (Level)	Impact Resistance (kg cm)	p
Epoxy-lacquer/Al	30	0.065	5.7	1	50	2.7×10^{-7}
PU/Cu	50	0.100	45.2	3	20	–
PU/(ball-milled Ag-Cu)	50	0.129	35.6	3	20	3.2×10^{-3}
PU/Al	40	0.068	38.3	1	40	8.6×10^{-6}
Aluminum/waterborne acrylic coating	30	0.113	7.7	0	15	3.0×10^{-1}

4. Conclusions

Orthogonal experiments showed that the infrared emissivity of coating was most significantly affected by drying time. In independent experiments, waterborne coatings with low infrared emissivity, low gloss, and low color difference were investigated by changing drying time. The results showed that when the drying time was 2.0 min, the gloss of waterborne coatings was lower, the infrared emissivity was lower, the color difference was small, the hardness was maximum, the adhesion was better (level 0), the impact resistance was the greater, the corrosion resistance was better, and performance of waterborne coating was better. Solving the corrosion resistance of waterborne coatings will be the future research direction. This work provides a new prospect for the industrial application of low infrared emissive coatings. It is suggested that the current results may be taken as the influence relationship of the studied factors.

Author Contributions: Conceptualization, Methodology, Validation, Resources, Data Curation, Writing—Original Draft Preparation, Supervision, X.Y.; Data Analysis, L.W. and X.Q.; Investigation, Writing—Review and Editing, L.W. All authors have read and agreed to the published version of the manuscript.

Funding: This research was funded by the Youth Science and Technology Innovation Fund of Nanjing Forestry University, grant number (CX2016018).

Conflicts of Interest: The authors declare no conflict of interest.

References

1. Wang, L.; Xu, G.Y.; Liu, C.Y.; Hou, H.L.; Tan, S.J. Surface-modified CeO₂ coating with excellent thermal shock resistance performance and low infrared emissivity at high-temperature. *Surf. Coat. Technol.* **2019**, *357*, 559–566. [[CrossRef](#)]
2. Tikum, A.F.; Kim, G.; Nasirian, A.; Ko, J.W.; Yoon, J.; Kim, J. Rhodamine-based near-infrared probe for emission detection of ATP in lysosomes in living cells. *Sens. Actuators B Chem.* **2019**, *292*, 40–47. [[CrossRef](#)]
3. Liang, J.; Li, W.; Xu, G.Y.; Meng, X.; Liu, K.; Tan, S.J. Preparation and characterization of the colored coating with low infrared emissivity based on nanometer pigment. *Prog. Org. Coat.* **2018**, *115*, 74–78. [[CrossRef](#)]
4. Ji, H.N.; Liu, D.Q.; Cheng, H.F.; Zhang, C.Y.; Yang, L.X. Vanadium dioxide nanopowders with tunable emissivity for adaptive infrared camouflage in both thermal atmospheric windows. *Sol. Energy Mater. Sol. Cells* **2018**, *175*, 96–101. [[CrossRef](#)]
5. Qiao, Z.; Mao, J. Multifunctional poly (melamine-urea-formaldehyde)/graphene microcapsules with low infrared emissivity and high thermal conductivity. *Mater. Sci. Eng. B Adv.* **2017**, *226*, 86–93. [[CrossRef](#)]
6. Zhao, J.; Luo, W.; Qi, L.; Yuan, L.; Huang, G.; Huang, Y.; Weng, X.L. The high-temperature resistance properties of polysiloxane/Al coatings with low infrared emissivity. *Coatings* **2018**, *8*, 125. [[CrossRef](#)]
7. Feng, G.J.; Li, Y.; Wang, Y.; Li, P.; Zhu, J.T.; Zhao, L. Ultrahigh infrared normal spectral emissivity of microstructured silicon coating Au film. *Opt. Lett.* **2012**, *37*, 299–301. [[CrossRef](#)]
8. Li, Q.Y.; Cheng, X.D.; Gong, D.Q.; Ye, W.P. Effect of N₂ flow rate on structural and infrared properties of multi-layer AlCrN/Cr/AlCrN coatings deposited by cathodic arc ion plating for low emissivity applications. *Thin Solid Films* **2019**, *675*, 74–85. [[CrossRef](#)]
9. He, L.H.; Zhao, Y.; Xing, L.Y.; Liu, P.G.; Zhang, Y.W.; Wang, Z.Y. Low infrared emissivity coating based on graphene surface-modified flaky aluminum. *Materials* **2018**, *11*, 1502. [[CrossRef](#)]
10. Xiong, X.Q.; Bao, Y.L.; Guo, W.J.; Fang, L.; Wu, Z.H. Preparation and application of high performance corn starch glue in straw decorative panel. *Wood Fiber Sci.* **2018**, *50*, 88–95.
11. Patel, R.; Kapatel, P. Waterborne polyurethanes: A three step synthetic approach towards environmental friendly flame retardant coatings. *Prog. Org. Coat.* **2018**, *125*, 186–194. [[CrossRef](#)]
12. Xu, W.; Wu, Z.H.; Zhang, J.L. Compressive creep and recovery behaviors of seat cushions in upholstered furniture. *Wood Fiber Sci.* **2015**, *47*, 431–444.
13. Xiong, X.Q.; Fang, L.; Wu, Z.H.; Zhang, M.; Lu, R.; Tetsuo, M. Special coating technology and film performance of rice straw particleboard. *J. Wood Fiber Sci.* **2016**, *72*, 139–146.
14. Izmitli, A.; Ngunjiri, J.; Lan, T.; Pacholski, M.L.; Smith, R.; Langille, M.; Roggow, T.; Henderson, K.; Kalantar, T.; Manna, J. Impact of silicone additives on slip/mar performance and surface characteristics of waterborne acrylic coatings. *Prog. Org. Coat.* **2019**, *131*, 145–151. [[CrossRef](#)]
15. Mirmohseni, A.; Gharieh, A.; Khorasani, M. Waterborne acrylic-polyaniline nanocomposite as antistatic coating: Preparation and characterization. *Iran. Polym. J.* **2016**, *25*, 991–998. [[CrossRef](#)]
16. Zhong, F.; He, Y.; Wang, P.Q.; Chen, C.L.; Lin, Y.; Wu, Y.Q.; Chen, J.Y. Self-assembled graphene oxide-graphene hybrids for enhancing the corrosion resistance of waterborne epoxy coating. *Appl. Surf. Sci.* **2019**, *488*, 801–812. [[CrossRef](#)]
17. Sabato, A.G.; Molin, S.; Javed, H.; Zanchi, E.; Boccaccini, A.R.; Smeacetto, F. In-situ Cu-doped MnCo-spinel coatings for solid oxide cell interconnects processed by electrophoretic deposition. *Ceram. Int.* **2019**, *45*, 19148–19157. [[CrossRef](#)]
18. Liu, Z.; Pan, Q.Q.; Xiao, C.F. Preparation and vacuum membrane distillation performance of a silane coupling agent-modified polypropylene hollow fiber membrane. *Desalination* **2019**, *468*, 114060. [[CrossRef](#)]
19. Chen, C.; Feng, X.M.; Shen, Y.F. Microstructures and properties of TiCp/Al coating synthesized on Ti-6Al-4V alloy substrate using mechanical alloying method. *J. Alloys Compd.* **2019**, *813*, 152223. [[CrossRef](#)]

20. Wang, H.J.; Chen, T.; Cong, W.L.; Liu, D.F. Laser cladding of Ti-based ceramic coatings on Ti₆Al₄V alloy: Effects of CeO₂ nanoparticles additive on wear performance. *Coatings* **2019**, *9*, 109. [[CrossRef](#)]
21. Liu, Y.F.; Xie, J.L.; Luo, M.; Jian, S.; Peng, B.; Deng, L.J. The synthesis and characterization of Al/Co₃O₄ magnetic composite pigments with low infrared emissivity and low lightness. *Infrared Phys. Technol.* **2017**, *83*, 88–93. [[CrossRef](#)]
22. Grossschartner, D.; Giesinger, I.; Doll, J.; Eyink, J. Highly versatile aluminum flake for water, solvent and ultra-low VOC coatings and inks. *CoatingsTech* **2018**, *15*, 22–28.
23. Yin, Y.J.; Zhou, S.X.; Gu, G.X.; Wu, L.M. Preparation and properties of UV-curable polymer/nanosized indium-doped tin oxide (ITO) nanocomposite coatings. *J. Mater. Sci.* **2007**, *42*, 5959–5963. [[CrossRef](#)]
24. GB/T 9754-2007 *Paints and Varnishes—Determination of Specular Gloss of Non-Metallic Paint Films at 20°, 60° and 85°*; Standardization Administration of the People’s Republic of China: Beijing, China, 2007; pp. 1–9. (In Chinese)
25. GB/T 1732-93 *Determination of Impact Resistance of Film*; Standardization Administration of the People’s Republic of China: Beijing, China, 1993; pp. 418–420. (In Chinese)
26. GB/T 1720-89 *Determination of Adhesion of Film*; Standardization Administration of the People’s Republic of China: Beijing, China, 1979; pp. 378–379. (In Chinese)
27. GB/T 6739-2006 *Paints and Varnishes—Determination of Film Hardness by Pencil Test*; Standardization Administration of the People’s Republic of China: Beijing, China, 2006; pp. 1–5. (In Chinese)
28. GB/T 3181-1995 *Colour Standard for Paint Film*; Standardization Administration of the People’s Republic of China: Beijing, China, 1995; pp. 10–17. (In Chinese)
29. GB/T 1731-93 *Determination of Flexibility of Films*; Standardization Administration of the People’s Republic of China: Beijing, China, 1993; pp. 414–415. (In Chinese)
30. GB/T 15748-2013 *The Method of Galvanic Corrosion Test for Metallic Ship Materials*; Standardization Administration of the People’s Republic of China: Beijing, China, 2013; pp. 1–5. (In Chinese)
31. Yan, X.X. Effect of black paste on the property of fluorine resin/aluminum infrared coating. *Coatings* **2019**, *9*, 597. [[CrossRef](#)]
32. Baneshi, M.; Maruyama, S.; Komiya, A. The effects of TiO₂ pigmented coatings characteristics on temperature and brightness of a coated black substrate. *Sol. Energy* **2012**, *86*, 200–207. [[CrossRef](#)]
33. Yan, X.X.; Xu, G.Y. Effect of surface modification of Cu with Ag by ball-milling on the corrosion resistance of low infrared emissivity coating. *Mater. Sci. Eng. B Adv.* **2010**, *166*, 152–157. [[CrossRef](#)]
34. Yan, X.X.; Xu, G.Y. Influence of silane coupling agent on corrosion-resistant property in low infrared emissivity Cu/polyurethane coating. *Prog. Org. Coat.* **2012**, *73*, 232–238. [[CrossRef](#)]
35. Yan, X.X.; Xu, G.Y. Corrosion and mechanical properties of polyurethane/Al composite coatings with low infrared emissivity. *J. Alloys Compd.* **2010**, *491*, 649–653. [[CrossRef](#)]
36. Yan, X.X.; Cai, Y.T.; Lu, R.; Miyakoshi, T. Development and characterization of new coating material of blended epoxy-lacquer with aluminum. *Int. J. Polym. Sci.* **2017**, *5017356*. [[CrossRef](#)]

